

# Click, Predict, Trust: Clinician-in-the-Loop AI Segmentation for Lung Cancer CT-Based Prognosis within the Knowledge-to-Action Framework

Mohammad R. Salmanpour<sup>1,2,3,\*</sup>, Sonya Falahati<sup>3</sup>, Amir Hossein Pouria<sup>4</sup>, Amin Mousavi<sup>5</sup>, Somayeh Sadat Mehrnia<sup>6</sup>, Morteza Alizadeh<sup>7</sup>, Arman Gorji<sup>3,8</sup>, Zeinab Farsangi<sup>9</sup>, Alireza Safarian<sup>9,10</sup>, Mehdi Maghsudi<sup>3</sup>, Carlos Uribe<sup>1,2,11</sup>, Arman Rahmim<sup>1,2,#</sup>, Ren Yuan<sup>2,11,#</sup>

<sup>1</sup>Department of Basic and Translational Research, BC Cancer Research Institute, Vancouver, BC, Canada

<sup>2</sup>Department of Radiology, University of British Columbia, Vancouver, BC, Canada

<sup>3</sup>Technological Virtual Collaboration (TECVICO Corp.), Vancouver, BC, Canada

<sup>4</sup>Amirkabir University of Technology, Department of Computer Engineering, Tehran, Iran

<sup>5</sup>Department of Computer, Abhar Branch, Islamic Azad University, Abhar, Iran

<sup>6</sup>Department of Integrative Oncology, Breast Cancer Research Center, Motamed Cancer Institute, ACECR, Tehran, Iran

<sup>7</sup>Department of Mathematics, University of Isfahan, Isfahan, Iran

<sup>8</sup>NAIRG, Department of Neuroscience, Hamadan University of Medical Sciences, Hamadan, Iran

<sup>9</sup>Rajaie Cardiovascular Medical and Research Center, Iran University of Medical Science, Tehran, Iran

<sup>10</sup>Department of Nuclear Medicine, University Hospital, Paracelsus Medical University, Salzburg, Austria

<sup>11</sup>BC Cancer, Vancouver Center, Vancouver, BC, Canada

\*Corresponding Author: [msalman@bccrc.ca](mailto:msalman@bccrc.ca)

#Co-Last-Authors

## ABSTRACT

**Objective:** Lung cancer is the leading cause of cancer death, with CT central to screening, prognosis, and treatment. Manual segmentation is variable and time-consuming, while deep learning offers automation but faces adoption barriers. Guided by the Knowledge-to-Action framework, this study develops a clinician-in-the-loop pipeline to improve reproducibility, prediction, and clinical trust.

**Methods:** Multi-center lung cancer CT data from 999 patients across 12 public datasets were analyzed. Five DL models (3D Attention U-Net, ResUNet, VNet, ReconNet, SAM-Med3D) were benchmarked against expert contours on whole and click-point cropped images. Segmentation reproducibility was tested with 497 PySERA-extracted radiomics features using Spearman correlation, ICC, Wilcoxon tests, and MANOVA. Prognostic modeling compared supervised (SL) and semi-supervised learning (SSL) with 38 dimensionality reduction strategies and 24 classifiers. Six physicians qualitatively evaluated masks across 21 questions spanning seven domains, including clinical meaningfulness, boundary quality, survival prediction, trust, and workflow integration.

**Results:** VNet-based segmentations achieved the best geometric accuracy (Dice  $0.83 \pm 0.07$ , IoU  $0.71 \pm 0.09$ ), radiomics stability (averaged correlation coefficient = 0.76, ICC = 0.65), and predictive performance under SSL (accuracy  $0.88 \pm 0.003$ , F1  $0.83 \pm 0.004$ ). SSL consistently outperformed SL across models. Radiologists favored VNet for peritumoral representation and smoother boundaries, while qualitative ratings showed no significant differences in diagnosis, prediction, or overall confidence. Importantly, experts preferred AI to provide initial masks for refinement rather than replace physicians.

**Conclusion:** This study shows that VNet, integrated with SSL, can deliver accurate, reproducible, and clinically trusted tools for CT-based lung cancer prognosis. Embedding AI as a supportive assistant within physician-centered workflows offers a feasible path to clinical translation.

**Keywords:** Lung Cancer CT Prognosis; Deep Learning Segmentation; Radiomics Analysis; Semi-Supervised Learning; Clinician-in-the-Loop AI; Knowledge-to-Action Framework

## 1. INTRODUCTION

For artificial intelligence (AI) in medical imaging to achieve clinical adoption, technical advances must be embedded within frameworks that address barriers to implementation [1]. The Knowledge-to-Action (KTA) framework within implementation science [2] provides such a roadmap, emphasizing that innovations must extend beyond methodological performance to overcome systemic, clinical, and workflow challenges. Previous studies [3-8] have highlighted the significant barriers to AI adoption in healthcare, including infrastructure issues, clinical skepticism, and the need for human-centered decision-making in AI applications. These findings align with the KTA framework's assertion that AI innovations must address both technical and systemic challenges. Our study further supports these conclusions by demonstrating how the KTA framework can guide AI integration, emphasizing the importance of addressing clinical workflows, reproducibility, and prediction performance in real-world settings. Our own prior work [2], specifically identified 11 barriers to AI diagnostic decision support tools adoption in diagnostic medicine: (i) infrastructure and integration, (ii) clinical skepticism and loss of human-centered decision-making, (iii) insufficient adaptability to clinical complexity, (iv) trust and accountability in AI-generated reporting, (v) ethical, legal, financial, and privacy concerns, (vi) lack of training and familiarity, (vii) workflow disruption and lack of standardization, (viii) workforce resistance due to job concerns, (ix) limitations in atypical or complex cases, (x) clinical distrust in AI decision-making, and (xi) bias, reliability, and quality challenges. Addressing these barriers is essential if AI is to move from promising prototypes to sustainable, evidence-based tools.

Lung cancer remains the leading cause of cancer-related mortality worldwide ( $>1.8$  million deaths annually) [9], with  $\sim 124,000$  deaths projected in the United States by 2025 [10]. Despite therapeutic advances, prognosis remains poor, underscoring the need for earlier detection, better prognostic assessment, and imaging-driven innovation—gaps aligned with KTA barriers of adaptability (iii) and workflow disruption (vii) [11, 12]. Large randomized trials—the U.S. National Lung Screening Trial (NLST) and the Dutch–Belgian NELSON trial—established low-dose CT as the only screening modality proven to reduce lung cancer mortality [13, 14]. Because CT is high-resolution, widely available, and relatively low cost, it is central to screening and follow-up, addressing infrastructure (i), workflow (vii), and clinical skepticism (ii) while mitigating financial concerns (v) [15]. Although PET/CT remains essential for staging [16], CT is the natural platform for embedding AI-enabled radiomics and prognostic pipelines [17, 18]. Ethical, legal, and privacy considerations (v) remain outside the scope of this work.

Segmentation remains a major bottleneck [18, 19]. Manual segmentation is subjective, time-intensive, and variable [20]. Fully automated deep learning (DL) models promise efficiency but lack generalizability across scanners, institutions, and tumor morphologies [21, 22], introducing risks: radiomic features become unstable, prognostic models irreproducible, and trust erodes [23]. Here, KTA barriers of adaptability (iii), trust (iv), clinical distrust (x), and reliability (xi) converge. Variability arises from observer differences, architectural diversity, irregular tumors, and multi-center heterogeneity [24, 25]. Left unresolved, these errors propagate into radiomics and outcome models [26]. Most prior studies relied on geometric scores such as Dice or Intersection over Union (IoU), without testing whether contours preserved radiomics stability or prognostic value [27], and limiting translation [28].

One solution is tumor-centered cropping with a peritumoral margin [29], which standardizes inputs, reduces irrelevant background, and preserves prognostically important peritumoral features. Technically, cropping lowers input size and memory demands, improving computational efficiency and lowering costs. Clinically, it enhances reproducibility across heterogeneous imaging. In KTA terms, cropping addresses infrastructure (i), adaptability (iii), workflow disruption (vii), and reliability (xi) [30]. Building on this, the study proposes a multi-pronged solution: (i) semi-automated segmentation with click-point or bounding-box guidance aligns physician oversight with algorithmic predictions, addressing workflow (vii) and skepticism (ii) [31, 32]; benchmarking five DL architectures across multi-center datasets evaluates reproducibility, addressing reliability (xi) and adaptability (iii) [30, 33]; radiomics stability analyses ensure features remain robust, targeting trust (iv) and clinical distrust (x) [24]; and (iv) expert qualitative review validates plausibility, countering skepticism (ii) and workforce resistance (viii) by showing AI supports rather than replaces clinicians [34].

Moving beyond Dice and IoU, which primarily assess the geometric fidelity of segmentation algorithms, radiomics analyses offer a radiologically meaningful evaluation [27]. They capture not only lesion size and shape but also intra-lesional textural heterogeneity, a feature highly sensitive to segmentation accuracy [35]. Outcome prediction further connects DL-based radiomics to patient survival, testing whether the generated contours encompass prognostically relevant regions [18, 36, 37]. By preserving radiomic features, such approaches retain subtle, prognostically informative signals; in atypical cases (ix), DL models can demonstrate that maintaining these features enhances outcome prediction, thereby strengthening clinical trust [38]. Still, prediction tasks face a scarcity of annotated outcome datasets [39]. Semi-supervised learning (SSL) addresses this by leveraging unlabeled data to improve generalization across multi-center cohorts [40, 41], lowering annotation burdens and addressing adaptability (iii) and lack of training/familiarity (vi) [42].

Quantitative radiomics metrics must be complemented by a qualitative physician-in-the-loop evaluation [42, 43], validating clinical plausibility and reinforcing interpretability [34]. A key principle is that AI should augment, not replace, clinical expertise [44]. DL can streamline segmentation, reduce variability, and enhance reproducibility, but physicians remain essential in oversight and decision-making [30]. Positioning AI as a clinical assistant addresses workforce resistance (viii) and strengthens trust (x) [32]. By showing how DL highlights subtle features while radiologists refine contours, this study reinforces the centrality of physician oversight [45].

Most prior work [23, 27, 46–48] stopped at geometric evaluation, rarely linking segmentation variability to radiomics reproducibility and survival, or embedding physician oversight. Few [29, 49] tested cropping, outcome-guided validation, or physician-in-the-loop review. The absence of these steps explains why DL segmentation, despite strong technical performance, has struggled with adoption [50, 51]. In the current study, we aim to fill that gap by integrating cropping, benchmarking, radiomics stability, outcome prediction, and physician-in-the-loop review within a single KTA-aligned framework. In doing so, it could address nearly all barriers to adoption, providing a roadmap for trustworthy AI in lung cancer imaging.

In summary, the current study makes four contributions (outlined next) that are aligned with KTA, tackling 10 of 11 above-mentioned barriers to adoption of AI: First, benchmarking five DL architectures for lung lesion segmentation across multi-center CT datasets tackles reliability (xi), adaptability (iii), and infrastructure (i). Second, radiomics stability analyses move beyond geometric accuracy to confirm prognostic preservation, aiming to better address clinical distrust (x). Third, a semi-automated, clinician-in-the-loop SSL framework reduces workflow disruption (vii), mitigates skepticism (ii), and lowers annotation burdens tied to training and familiarity (vi). Fourth, comparing grand truth- and DL-based radiomics features in ML classification with physician review explains when DL performs better or worse, addressing

variability (xi), atypical cases (ix), and workforce resistance (viii) by confirming AI's role as assistant, not replacement. While this study tackles nearly all KTA barriers, ethical, legal, financial, and privacy concerns (v) remain beyond the scope and require institutional and policy solutions. Collectively, these contributions demonstrate not only technical feasibility but also a barrier-focused pathway for embedding AI into clinical practice.

## 2. METHOD AND MATERIAL

**i) Patient/Imaging Data.** Clinical data, CT scans, and manually delineated lesion masks (described in Section (iv)) were obtained from 999 patients out of a total of 2,092 across 12 publicly and privately available datasets, all accessed through The Cancer Imaging Archive (TCIA). The included datasets were: LCTSC (35 out of 60 patients) [52], LIDC-IDRI (289 out of 1010 patients) [53], Lung-Fused-CT-Pathology (6 patients) [54], LungCT-Diagnosis (49 out of 61 patients) [55], NSCLC-Radiogenomics (39 out of 211 patients) [56], NSCLC-Radiomics (417 out of 422 patients) [57], NSCLC-Radiomics-Genomics (53 out of 89 patients) [58], QIN Lung CT (38 out of 47 patients) [59, 60], RIDER Lung CT (12 out of 32 patients) [61], RIDER Pilot (4 out of 8 patients) [62], SPIE-AAPM Lung CT Challenge (44 out of 77 patients) [63], and TCGA-LUAD (13 out of 69 patients) [64]. Demographic and clinical characteristics varied across datasets. Patient demographics and clinical characteristics varied considerably across datasets. For example, the Lung-Fused-CT-Pathology cohort comprised 83.3% males with a mean age of  $74.8 \pm 10.3$  years and a mean tumor size of  $12.2 \pm 1.9$  mm. The NSCLC-Radiomics dataset included 72.3% males (mean age:  $66.2 \pm 10.3$  years) with histological subtypes of squamous cell carcinoma (50.2%), large cell carcinoma (30.1%), adenocarcinoma (12.3%), and NOS/NA (7.4%). The LungCT-Diagnosis dataset contained 59.6% of patients aged  $\geq 65$  years, with 53.2% males predominantly diagnosed at advanced stages (III/IV). In addition, patients across all datasets were stratified into prognostic groups based on overall survival (OS): Class 1 (survival  $> 4$  years) representing a favorable prognosis, and Class 0 (survival  $< 4$  years) representing a poor prognosis. By integrating 12 heterogeneous, multi-center datasets with diverse demographics, tumor subtypes, and outcome profiles, this study directly addresses KTA barriers of insufficient adaptability to clinical complexity (iii), bias and reliability challenges (xi), and infrastructure and integration (i) by ensuring that the developed framework is tested across varied real-world conditions rather than narrow, single-center cohorts.

**ii) Mask Delineation and Expert Verification.** Chest CT scans were first assessed in the standard lung window with multiplanar reconstructions to identify nodules displaying features suspicious for malignancy, such as irregular morphology, spiculated or lobulated margins, abnormal attenuation, or rapid growth. Lesions deemed suspicious were manually segmented on each axial slice in 3D Slicer (v5.8) by two board-certified diagnostic physicians (thoracic radiology) working in consensus, adhering to a prespecified image-based lung-tumor contouring protocol; pathology/MTB, when available, was used only to confirm lesion identity and did not alter boundaries. To ensure consistency and reduce annotation errors, all segmentation masks were subsequently reviewed and confirmed by one independent clinical expert. This dual-review protocol was adopted to strengthen inter-observer reliability and to ensure accurate lesion localization, which is essential for downstream radiomics feature extraction. Cases with compromised boundary definition—caused by pleural effusion, bulky lymphadenopathy, atelectasis, extensive fibrosis, or other confounding pathology—were excluded from further analysis. This expert-driven, consensus-based protocol directly addresses KTA barriers of clinical skepticism (ii), adaptability to clinical complexity (iii), and reliability and quality challenges (xi) by ensuring that only high-quality, clinically validated masks advance to radiomics analysis.

**iii) Preprocessing and ROI-Based Cropping for Tumor-Focused Segmentation.** All 3D CT volumes and corresponding masks were standardized using a multi-step preprocessing pipeline. CT scans were z-score normalized on a per-volume basis (mean/standard deviation), and masks were binarized to [0,1]. Volumes were resampled to  $64 \times 64 \times 64$  voxels using trilinear interpolation to ensure consistency and computational efficiency. A tumor-centered region-of-interest (ROI) cropping strategy preserved the largest connected component with a 5-voxel 3D margin, thereby retaining peritumoral context while minimizing background. Cropping was performed with SimpleITK, with updated origins and complete logs maintained for reproducibility. This preprocessing enhanced signal-to-noise ratio, reduced irrelevant regions, and improved segmentation performance across all 3D DL models while preserving geometric fidelity [65]. This preprocessing and tumor-centered cropping strategy directly addresses KTA barriers of infrastructure and integration (i), adaptability to clinical complexity (iii), workflow disruption (vii), and reliability and quality challenges (xi) by standardizing inputs, reducing computational burden, and ensuring reproducible, tumor-focused segmentation across multi-center datasets.

**iv) DL Segmentation Networks.** The choice of 3D Attention U-Net [66], ResUNet [67], V-Net [68], ReconNet [67], and SAM-Med3D [69] was motivated by their complementary architectures and demonstrated success in medical image segmentation. 3D Attention U-Net employs attention mechanisms for improved boundary localization, ResUNet leverages residual connections for stable optimization, and V-Net is a widely validated 3D model for volumetric CT imaging. ReconNet provides a lightweight and efficient alternative, while SAM-Med3D introduces recent advances in foundation models with strong generalization capabilities [67]. To ensure robustness, these networks were applied to both whole CT images and cropped (click-point-guided) tumor-centered volumes, enabling a direct evaluation of segmentation variability

under different input strategies. Ten independent datasets, including LCTSC, LIDC-IDRI, Lung-Fused-CT-Pathology, NSCLC-Radiogenomics, NSCLC-Radiomics, QIN Lung CT, RIDER Lung CT, RIDER Pilot, SPIE-AAPM Lung CT Challenge, and TCGA-LUAD, were used for training each network, with approximately 72% of cases allocated for training and 18% for validation. Model selection was based on validation performance, and generalizability was further assessed through external testing on two independent datasets, such as LungCT-Diagnosis and NSCLC-Radiomics-Genomics (~10%). Segmentation performance was measured using the Dice similarity coefficient, IoU, and Hausdorff distance, all computed via the AllMetrics library, which standardizes machine learning evaluation [70]. This was essential, as recent studies [71] have shown significant discrepancies in metric values across platforms (MATLAB, Python, R) and even across different Python libraries, raising concerns about reproducibility. Using AllMetrics ensured consistent, transparent, and comparable results. By selecting well-established networks and standardized evaluation, this step addresses KTA barriers of adaptability to clinical complexity (iii), reliability and quality challenges (xi), and lack of training or familiarity with AI tools (vi), while enhancing trust among clinical professionals.

**v) Radiomics Feature Extraction and Normalization.** All CT scans underwent quality control to ensure they were free of artifacts before preprocessing. Lung cancer lesions were manually segmented in 3D Slicer by two trained physicians and subsequently reviewed by one experienced thoracic medical expert for accuracy. A total of 497 radiomics features were extracted from each ROI, including both the ground truth annotations segmented by medical professionals and the masks generated by the five DL networks, using the PySERA library within VisERA 1.0 software, which is extensively standardized in accordance with the Image Biomarker Standardization Initiative [72]. The extracted radiomic features are categorized into three major groups: 50 first-order intensity features, which capture basic statistics such as mean, variance, skewness, and kurtosis (including subsets of local intensity, intensity-based statistics, intensity histogram, and intensity-volume histogram); 29 shape and morphological features, which quantify geometric characteristics such as volume, surface area, compactness, and sphericity; and 408 texture features, which describe spatial intensity patterns and intra-tumoral heterogeneity. The texture group is further divided into 150 Gray-Level Co-occurrence Matrix (GLCM) features, 96 Gray-Level Run Length Matrix (GLRLM) features, 48 Gray-Level Size Zone Matrix (GLSZM) features, 48 Gray-Level Distance Zone Matrix (GLDZM) features, 15 Neighborhood Gray-Tone Difference Matrix (NGTDM) features, 51 Neighboring Gray-Level Dependence Matrix (NGLDM) features, and 10 moment-invariant features. All features were normalized using min–max scaling to ensure comparability across datasets, prevent bias from differing feature ranges, and improve the stability and convergence of downstream classification analysis. Among the 12 datasets, only NSCLC-Radiogenomics, LungCT-Diagnosis, and NSCLC-Radiomics included documented OS data, comprising a total of 499 patients, while the remaining datasets were incorporated exclusively into the SSL framework. Both SL and SSL approaches were applied across multiple ML models to predict OS in patients with NSCLC. This step directly addresses KTA barriers of trust and accountability (iv), reliability and quality challenges (xi), adaptability to clinical complexity (iii), clinical distrust in AI decision-making (x), and workflow disruption/lack of standardization (vii), ensuring that radiomics analyses remain reproducible, interpretable, and clinically relevant.

**vi) Statistical Radiomics Assessment.** Radiomics features extracted from DL-generated masks were compared to those from ground truth using Spearman correlation and paired t-tests to assess reproducibility, stability, and systematic bias due to segmentation variability. Radiomics captures tumor size, shape, higher-order textural patterns, and intratumoral heterogeneity, all of which are sensitive to segmentation differences. Ensuring that DL contours preserve these features is essential for maintaining prognostic reliability and preventing variability from impacting outcome models. To evaluate normality, the Shapiro-Wilk test was applied, categorizing the data as "Normal" or "Not normal" based on the p-value. The Spearman correlation coefficient assessed the strength and direction of monotonic relationships between variables, while the Intraclass Correlation Coefficient (ICC) measured the consistency or reproducibility of the measurements. For non-normally distributed data, the Wilcoxon signed-rank test was used to compare paired samples. MANOVA was performed on multivariate data, with Wilks' lambda, Pillai's trace, Hotelling-Lawley trace, and Roy's greatest root reported to test group differences. The paired t-test was used for normally distributed data to identify significant variations between groups, reporting the t-value and the number of significant differences. Combining these methods allows for a rigorous evaluation of DL-based radiomics beyond correlation alone. This analysis directly addresses KTA barriers of trust and accountability (iv), variability and reliability (xi), workflow integration (vii), and clinician skepticism (ii). At the conclusion of this step, DL-generated masks are expected to show strong concordance with expert annotations. If discrepancies are found, further qualitative review and downstream classification or survival modeling will be performed to investigate and explain any variations. This framework strengthens the study's robustness and provides a generalizable model for assessing segmentation reliability across cancers and imaging modalities, advancing the integration of AI into clinical imaging practice.

**vii) Machine Learning Classification Analysis.** We employed two complementary frameworks: supervised learning (SL) and SSL. In the SL framework, the labeled NSCLC-Radiomics dataset was partitioned into five folds. In each iteration, four folds were used for training and one for validation, ensuring that every fold served once as the validation set. To assess generalizability, models trained on each fold were also tested on two independent external datasets—NSCLC-

Radiogenomics and LungCT-Diagnosis. Performance metrics included Accuracy, Precision, Recall, F1 -score, Receiver Operating Characteristic–Area Under the Curve (ROC-AUC), and Specificity, reported as mean  $\pm$  standard deviation across folds and external sets. Final model selection was based on the best overall performance validated externally. In the SSL framework, the NSCLC-Radiomics dataset was again split into five folds. A logistic regression (LR) model trained on four folds generated pseudo-labels for the unlabeled datasets (including the LCTSC, LIDC-IDRI, Lung-Fused-CT-Pathology, NSCLC-Radiogenomics, QIN Lung CT, RIDER Lung CT, RIDER Pilot, SPIE-AAPM Lung CT Challenge, and TCGA-LUAD). The held-out fold was excluded from pseudo-labeling to avoid bias and data leakage. The model was then retrained on the combined labeled and pseudo-labeled data and evaluated on the excluded fold as well as the two external test sets. By leveraging unlabeled data, this framework improved model generalization across centers and patient populations, complementing the SL framework.

To address the high dimensionality of radiomics features and reduce overfitting, dimensionality reduction strategies were applied, including feature selection algorithms (FSAs) and automated embedding algorithms (AEAs), totaling 38 approaches. FSAs covered filter-based methods (e.g., Chi-Square Test, Correlation Coefficient [CC], Mutual Information [MI], Information Gain (IG), Mutual Information Gain Ratio (MIGR)), statistical tests (e.g., Analysis of Variance [ANOVA] F-Test, Chi-Square P-value, Variance Thresholding [VT]), wrapper-based approaches (e.g., Recursive Feature Elimination [73], Sequential Forward Selection [SFS], Sequential Backward Selection [SBS]), embedded methods (e.g., Least Absolute Shrinkage and Selection Operator [Lasso], Elastic Net [ENet], Stability Selection), and ensemble strategies (e.g., Random Forest Importance [RF-Imp], Extra Trees [ETI], Permutation Importance [Perm-Imp]). Additional statistical controls, such as False Discovery Rate (FDR), Family-Wise Error (FWE), and Variance Inflation Factor (VIF), were also incorporated.

The AEAs (19 methods) provided complementary transformations, including Principal Component Analysis (PCA), Kernel PCA (K-PCA), Independent Component Analysis (ICA/FastICA), Factor Analysis, Non-Negative Matrix Factorization (NMF), and nonlinear manifold learning methods such as t-distributed Stochastic Neighbor Embedding (t-SNE), Uniform Manifold Approximation and Projection (UMAP), Isomap, Locally Linear Embedding (LLE), Spectral Embedding, Multidimensional Scaling (MDS), and Diffusion Maps. Deep learning–based autoencoders (AE), as well as Feature Agglomeration, Truncated Singular Value Decomposition (SVD), and random projection techniques (Gaussian Random Projection (GRP) and Sparse Random Projection (SRP)), were also used for scalable dimensionality reduction. Each reduced feature set was evaluated with a comprehensive panel of 24 classifiers representing linear, probabilistic, kernel-based, tree-based, neural, and ensemble learning methods. These included Logistic Regression (LR), Linear Discriminant Analysis (LDA), Naïve Bayes (Gaussian [GNB], Bernoulli [BNB], Complement variants [CNB]), Support Vector Machines (SVMs) with multiple kernels, k-Nearest Neighbors (k-NN), Decision Trees (DT), Random Forest (RF), Extra Trees (ET), Gradient Boosting (GB), AdaBoost (AB), HistGradient Boosting (HGB), Light Gradient Boosting Machine (LGBM), Extreme Gradient Boosting (XGBoost), and Multi-Layer Perceptrons (MLP). Meta-ensembles such as Stacking, Voting (VC), and Bagging further enhanced predictive robustness. Additional classifiers included Nearest Centroid (NC), Gaussian Process Classifier (GPC), Decision Stump (DS), Dummy Classifier (DC), and Stochastic Gradient Descent Classifier (SGDC). Hyperparameters were optimized via five-fold cross-validation and grid search.

By combining SL and SSL frameworks, dimensionality reduction, and a broad classifier panel validated on external datasets, this analysis ensured robustness, reproducibility, and interpretability. Importantly, this classification analysis also served as a direct evaluation of DL-generated masks compared with expert ground truth annotations. By testing whether radiomics features derived from DL masks achieve comparable or superior predictive performance relative to physician-delineated contours, the framework identified where DL masks performed better or worse than expert ground truth in both prediction and diagnostic tasks. Following this analysis, physicians with expertise in AI, radiomics, and ML-based classification reviewed the results to investigate why such differences occurred. This included examining what regions DL algorithms prioritized during segmentation, which prognostic features they captured, and what subtle information clinicians may have missed but DL models detected. Conversely, cases where DL performed worse were analyzed to reveal algorithmic limitations or overlooked tumor regions. Such physician-in-the-loop interpretation is not only about validating DL outputs but also about revealing how much margin or peritumoral region clinicians may need to consistently include for reliable diagnosis and prediction. In alignment with the KTA framework, this classification analysis addressed barriers of adaptability (iii), variability and reliability (xi), limitations in atypical or complex cases (ix), and workforce resistance (viii) by demonstrating that DL models can complement rather than replace clinical expertise.

**viii) Qualitative review Analysis.** In this section, six physicians assessed the masks generated by DL models, comparing them to the ground truth annotations. Three physicians contributed to manual segmentation for the ground truth, while three external physicians validated the AI-generated masks. The evaluation involved comparing the outputs of five DL models to the ground truth and extracting radiomic features from ROIs for survival prediction tasks. This analysis summarizes key evaluation areas, including tumor delineation, spatial differences, and the clinical relevance of AI mask deviations for prognosis and survival prediction. The evaluation protocol spanned seven domains with 21 questions, as listed in Supplemental File 1. In (q1), radiologists judged whether AI masks defined tumor volumes as more clinically

meaningful than ground truth. (q2) asked if AI–ground truth differences were concentrated in the peritumoral zone, while (q3) evaluated the clinical meaningfulness or justification of those differences. (q4) assessed preservation of internal tumor heterogeneity, and (q5) focused on boundary quality. Prognostic value was examined in (q6), asking whether AI–ground truth differences captured survival-relevant tissue, and in (q7), whether deviations in tumor volume were harmful or beneficial for prediction. Trust and preference were probed in (q8), addressing the likelihood that AI masks could outperform ground truth in subtle cases, and in (q9), whether experts would prefer AI masks for survival prediction tasks. Overall assessments included (q10) diagnostic success, (q11) prognostic success, (q12) confidence in evaluation, (q13) sufficiency of geometric metrics, and (q14) identification of additional evaluation needs. Workflow and adoption were explored in (q15) usability, (q16) clinical actionability, (q17) robustness, (q18) time-saving potential, (q19) trust in high-stakes clinical tasks, and (q20) the value of confidence maps. Finally, (q21) captured expert opinion on the broader role of AI in clinical practice—whether to replace physicians, provide initial masks for refinement, or act as a supportive tool. By embedding physician expertise in this way, the analysis strengthens transparency, clinical trust, and interpretability, addressing KTA barriers of clinical skepticism (ii), distrust in AI decision-making (x), and workforce resistance (viii).

### 3. RESULTS

#### 3.1 Lesion Segmentation Results

As shown in Figure 1, V-Net on cropped (click-point) images consistently outperforms the other models, all in terms of Dice score, Hausdorff Distance, and IoU, particularly in both the test and validation datasets. In the test dataset, VNet achieves the highest values for both metrics (Dice:  $0.83 \pm 0.07$ , IoU:  $0.71 \pm 0.09$ ), with the lowest Hausdorff Distance ( $10.04 \pm 3.73$ ). In the validation set, VNet also shows top performance (Dice:  $0.77 \pm 0.15$ , IoU:  $0.64 \pm 0.16$ , Hausdorff Distance:  $11.66 \pm 5.50$ ). The difference in testing performance between VNet and the other networks is statistically significant ( $p < 0.05$ , paired t-test with Benjamini-Hochberg False Discovery Rate correction). ReconNet performs well in the test set with a Dice score of  $0.79 \pm 0.11$  and IoU of  $0.67 \pm 0.13$ , showing a Hausdorff Distance of  $11.39 \pm 3.96$ . In the validation set, it slightly underperforms (Dice:  $0.72 \pm 0.17$ , IoU:  $0.59 \pm 0.18$ , Hausdorff Distance:  $13.17 \pm 5.42$ ). ResUNet performs moderately in both datasets. In the test set, it shows a Dice score of  $0.75 \pm 0.09$  and an IoU of  $0.61 \pm 0.10$ , with a Hausdorff Distance of  $19.91 \pm 6.91$ . In the validation set, its performance drops slightly (Dice:  $0.74 \pm 0.10$ , IoU:  $0.60 \pm 0.12$ , Hausdorff Distance:  $20.17 \pm 7.73$ ). 3D Attention U-Net, though providing competitive performance in the test set (Dice:  $0.77 \pm 0.08$ , IoU:  $0.64 \pm 0.10$ ), exhibits a significantly higher Hausdorff Distance ( $33.61 \pm 4.10$ ) compared to the other models, indicating more variability in boundary predictions. In the validation set, its performance remains consistent (Dice:  $0.76 \pm 0.11$ , IoU:  $0.63 \pm 0.13$ , Hausdorff Distance:  $33.48 \pm 4.40$ ). SAM-Med3D demonstrates the lowest performance in both Dice score and IoU, particularly in the validation set (Dice:  $0.61 \pm 0.27$ , IoU:  $0.49 \pm 0.24$ ). In the test set, it has a relatively lower Hausdorff Distance ( $4.13 \pm 1.55$ ) but performs poorly in accurate metrics. Moreover, all networks trained on whole images underperformed compared to cropped images, yielding significantly lower results (Dice:  $0.30$ , IoU:  $0.20$ , Hausdorff Distance:  $9$ ;  $p < 0.001$ , paired t-test with Benjamini-Hochberg FDR correction). In conclusion, VNet emerges as the most robust model in both testing and validation, offering a balance of high accuracy (Dice and IoU) and low boundary variability (Hausdorff Distance), with its performance being significantly superior to the other networks. The hyperparameters and architectural characteristics of the DL models are provided in Supplemental File 2.

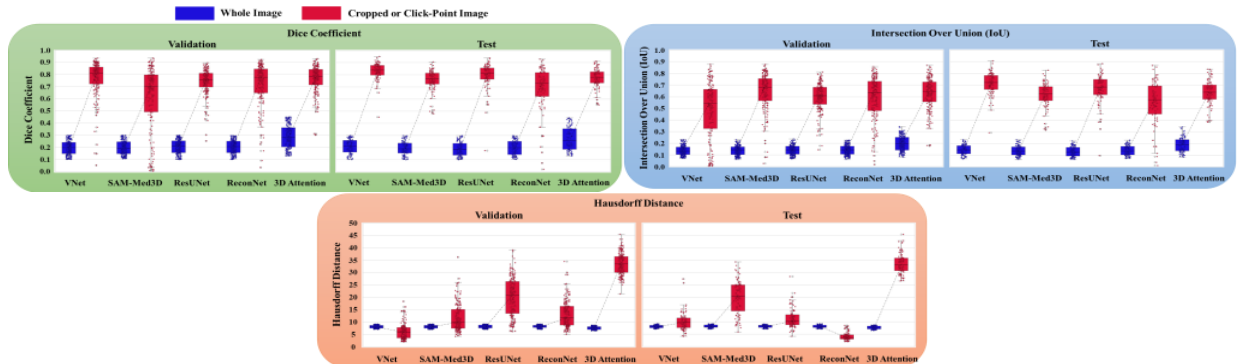


**Figure 1.** Comparative performance of five lung lesion segmentation models on whole (blue) vs. cropped (red) CT images.

#### 3.2 Statistical Radiomics Assessment Results

As shown in Table 1, the statistical analysis of radiomics features extracted from the DL-generated masks revealed strong performance across all evaluated models, with V-Net demonstrating the most consistent results. The Spearman correlation coefficients ( $\rho$ ) demonstrated a consistent monotonic relationship between the DL-derived and ground truth features, ranging from 0.72 to 0.76, with V-Net achieving the highest correlation at 0.76, indicating the strongest alignment. The ICC values, which assessed reproducibility, ranged from 0.61 to 0.67, with V-Net showing a high ICC of 0.65, reflecting

moderate to high consistency. Non-normal data distributions were assessed using the Wilcoxon signed-rank test (W), where lower W values indicate greater significance. As shown, significant differences were observed in all models, with V-Net demonstrating a small W value (89.71) after 3D Attention U-Net (69.83), indicating the most pronounced differences. MANOVA analysis further confirmed multivariate differences across all models, with lower Wilks'  $\lambda$  indicating greater group differences (V-Net had a value of 0.02), and higher Pillai's trace (V-Net: 0.98), Hotelling-Lawley trace (V-Net: 58.57), and Roy's greatest root (V-Net: 58.57), suggesting robust statistical significance in V-Net. Notably, 3D Attention U-Net performed similarly to V-Net, showing values close to V-Net across these metrics, though still slightly lower in terms of significance. Paired t-test results for normally distributed features showed that variations between models and ground truth were generally small, with the number of significant differences ranging from 26 to 97 out of 497 total radiomics features. V-Net and 3D Attention U-Net exhibited the fewest significant differences ( $p < 0.05$ , paired t-test). These findings underscore the reliability of V-Net-generated masks for radiomics analysis, though further qualitative review is necessary to investigate discrepancies and ensure model robustness in clinical applications. Calculated values for each statistical test are provided in Supplemental File 3.

**Table 1.** Statistical analyses of radiomics features extracted from the DL-generated masks, compared to the ground truth (GT). ICC: Intraclass Correlation Coefficient.

Method	Test Type	ReconNet	ResUNet	VNet	3D Attention	SAM-Med3D
Shapiro (Normal/Not-normal)	Ground Truth (314/183)	331/166	282/215	364/133	298/199	340/157
Spearman	Correlation Coefficient	0.72	0.76	0.76	0.76	0.74
ICC	Coefficient	0.62	0.65	0.65	0.61	0.67
Wilcoxon	Coefficient	94.21	123.01	89.71	69.83	105.52
	Wilks' $\lambda$	0.04	0.02	0.03	0.02	0.04
	Pillai's Trace	0.96	0.98	0.97	0.98	0.96
MANOVA	Hotelling-Lawley Trace	21.59	57.23	37.00	58.57	21.47
	Roy's Greatest Root	21.59	57.23	37.00	58.57	21.47
	Decision	Rejected	Rejected	Rejected	Rejected	Rejected
Paired t-test	Number of Significant differences/ 497 total features	83/498	97/498	36/497	26/498	49/498

### 3.3 Prediction Analysis

In 5-fold cross-validation (Figure 2), SSL consistently outperformed SL, achieving higher accuracy, recall, and F1-scores with tighter deviations, while SL showed more variability. For instance, SSL with MI-MLP-ResUNet reached  $0.88 \pm 0.003$  accuracy,  $0.88 \pm 0.003$  recall, and  $0.83 \pm 0.004$  F1, compared to  $0.75 \pm 0.005$ ,  $0.75 \pm 0.005$ , and  $0.64 \pm 0.007$  for SL, with similar advantages observed for MIGR-ET-ground truth and ReliefF-GB-SAM-Med3D. The LASSO-LGBM-VNet configuration stood out, consistently achieving the strongest validation results ( $0.88 \pm 0.003$  accuracy,  $0.83 \pm 0.004$  F1, and  $0.65 \pm 0.031$  AUC), confirming the power of VNet as a segmentation backbone. Independent test evaluations supported these findings, though SSL-SL gaps were narrower: while models like MI-MLP-ResUNet and ReliefF-GB-SAM-Med3D showed similar performances across paradigms, VNet again demonstrated clear superiority. Under SSL, LASSO-LGBM-VNet achieved the highest test accuracy ( $0.88 \pm 0.000$ ) and a strong AUC ( $0.76 \pm 0.048$ ), whereas its SL counterpart, despite maintaining accuracy ( $0.87 \pm 0.012$ ), dropped sharply in AUC ( $0.40 \pm 0.058$ ) ( $p < 0.05$ , paired t-test with Benjamini-Hochberg False Discovery Rate correction). Likewise, GRP-VC-3D Attention further highlighted SSL's advantage, achieving  $0.81 \pm 0.025$  accuracy and  $0.82 \pm 0.029$  F1, while SL lagged at  $0.72 \pm 0.079$  accuracy and  $0.75 \pm 0.062$  F1.

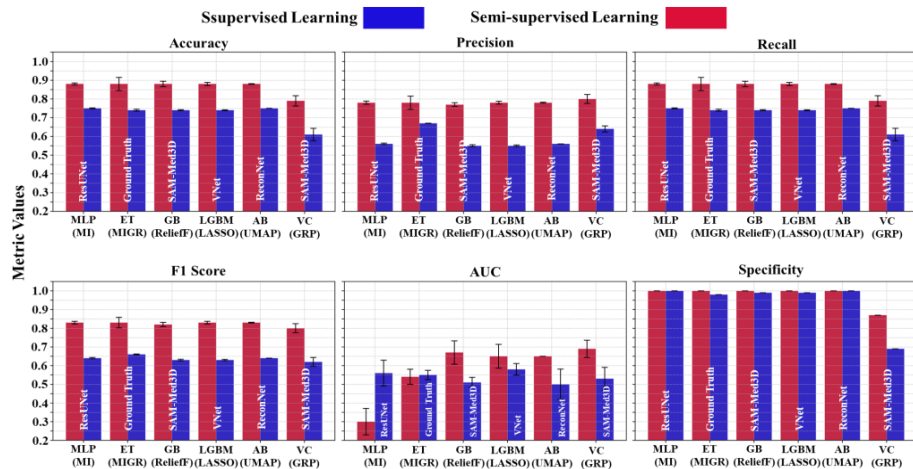


**Figure 2.** Five-fold cross-validation performance of classification pipelines based on radiomics features extracted from segmentation masks generated by five models and Ground-Truth masks. Red bars correspond to semi-supervised learning and blue bars to supervised learning, with error bars showing standard deviation across folds.

Taken together, the cross-validation and independent test results demonstrate that SSL provides significantly more stable and reliable predictive performance compared to SL. SSL models consistently achieved higher accuracy, recall, and F1-scores while also sustaining stronger AUC and specificity, particularly in configurations involving LASSO–LGBM–VNet and MIGR–ET–ground truth. Importantly, VNet stood out as the most powerful backbone among the segmentation models, delivering superior performance across both validation and test phases and showing greater robustness in SSL than in SL. While SL occasionally approached SSL on the test set (e.g., ReliefF–GB–SAM-Med3D and UMAP–AB–ReconNet), it was generally associated with larger standard errors and less consistent generalization. These findings collectively highlight both the overall robustness of SSL and the particularly strong role of VNet in driving state-of-the-art classification outcomes. The hyperparameters, architectural characteristics, selected features, and results of five-fold cross-validation and external tests for the FSAs/AEAs combined with classifiers on each dataset, using radiomics features extracted from DL-generated masks and ground truth, are provided in Supplemental Files 4–15.

### 3.4 Qualitative Visual Assessment

Six board-certified thoracic radiologists (5–15 years of experience) independently evaluated segmentation masks from five models. The heatmap in Table 2 summarizes average Likert ratings across 20 scored questions (q1–q13, q15–q20), with q14 excluded as descriptive and q21 treated as categorical. For most items, higher scores indicated more favorable outcomes, except for q5 (boundary noisiness), where lower scores were preferable. For q21 (Role of AI in clinical practice), radiologists selected among three options: Option A — Replace physicians entirely, Option B — Provide an initial mask for physicians to refine, or Option C — Assist physicians as a support/check tool.

Section 1 — Overall Impression (q1): Ratings were modest ( $\approx 2.2$ – $2.8$ ), indicating that AI masks were not consistently judged more clinically meaningful than ground truth. (Descriptive only).

Section 2 — Spatial Differences (q2–q3): Peritumoral concentration (q2, higher = better) scored highest for 3DAttention and VNet ( $\approx 3.8$ ), while the clinical meaningfulness of differences (q3, higher = better) also favored these models ( $\approx 3.5$ ) compared to SAM-Med3D ( $\approx 1.5$ ). (Descriptive only).

Section 3 — Tumor Heterogeneity & Boundary Quality (q4–q5): Preservation of heterogeneity (q4, higher = better) was moderate ( $\approx 2.7$ – $3.5$ ). Boundary quality (q5, lower = better) showed that 3DAttention and VNet produced smoother, less noisy contours ( $\approx 2.7$ ), whereas other models demonstrated greater noisiness. (Descriptive only).

Section 4 — Survival Prediction Relevance (q6–q7): Scores were mid-range ( $\approx 2.3$ – $3.0$ , higher = better), suggesting that AI–ground truth deviations were somewhat prognostically relevant but not strongly impactful. (Descriptive only).

Section 5 — Trust & Preference (q8–q9): Ratings were modest ( $\approx 1.7$ – $2.7$ , higher = better), reflecting limited clinician preference for adopting AI masks over ground truth in survival prediction tasks. (Descriptive only).

Section 6 — Summaries & Overall Assessment (q10–q13): Diagnostic and prognostic success (q10–q11, higher = better) were moderate ( $\approx 2.7$ – $3.5$ ). Friedman tests revealed no statistically significant differences among the five models in diagnosis-oriented evaluation (q10:  $\chi^2 = 2.140$ ,  $p = 0.710$ ) or prediction-oriented evaluation (q11:  $\chi^2 = 3.802$ ,  $p = 0.433$ ). Overall confidence (q12, higher = better) reached some of the strongest values (up to 4.0).

Sufficiency of geometric metrics (q13, higher = better) was consistently low ( $\approx 2.2$ – $2.3$ ), and the Friedman test again confirmed no significant differences among models ( $\chi^2 = 1.714$ ,  $p = 0.788$ ). A global Friedman test of overall ratings also showed no significant differences ( $\chi^2 = 4.205$ ,  $p = 0.379$ ). For q14, physicians agreed that trustworthy AI segmentation requires evaluations beyond geometric accuracy, emphasizing clinical review, radiomics stability, survival prediction, workflow impact, and robustness to noise. They considered these more effective than Dice or IoU alone, as they better connect segmentation to clinical outcomes, usability, and real-world trust.

Section 7 — Workflow & Adoption (q15–q20, q21): Usability (q15), clinical actionability (q16), robustness (q17), and time-saving potential (q18) showed mixed results. Usability and actionability scored moderate ( $\approx 2.5$ – $3.7$ ), robustness was mid-range ( $\approx 3.0$ – $3.3$ ), while time-saving potential was consistently the lowest ( $\approx 1.0$ – $1.8$ ). By contrast, trust in high-stakes tasks (q19) and interpretability via confidence maps (q20) scored highly ( $\approx 4.2$ – $4.4$ ), emphasizing the importance of transparency for clinical acceptance. For q21 (categorical), radiologists confirmed that AI should provide an initial mask for refinement or serve as a supportive tool, rather than replace physicians. Friedman tests were formally applied to overall ratings and selected domain-specific items (q10, q11, q13). All results were non-significant (all  $p > 0.3$ ), indicating no systematic differences among the five models in these domains. The remaining questions (q1–q9, q12, q15–q20, q21) were analyzed descriptively. Their distributions showed consistent patterns across models, with no evidence of divergent performance. Collectively, these findings support the conclusion that, from a clinical perspective, the five models offer equivalent clinical utility despite differences in technical segmentation metrics. Qualitative assessments are provided in Supplemental File 16.

**Table 2.** Heatmap of qualitative evaluation results derived from physicians for masks segmented by deep learning algorithms.

Question	q1	q2	q3	q4	q5	q6	q7	q8	q9	q10	q11	q12	q13	q15	q16	q17	q18	q18	q20	q21
<b>3DAttention</b>	2.8	3.8	3.5	3.2	3.5	2.8	3.0	2.7	2.3	3.5	2.6	3.7	2.3	3.2	3.7	3.3	4.2	1.7	4.2	2.4
<b>SAM-Med3D</b>	2.2	2.0	1.5	1.8	2.0	1.8	2.7	1.8	1.7	2.5	1.8	4.0	2.3	2.5	3.5	2.7	3.3	1.0	4.2	2.5
<b>ReconNet</b>	2.2	2.7	3.0	2.7	2.5	2.3	2.2	2.0	2.0	3.3	2.4	3.7	2.3	3.3	2.8	3.0	4.2	1.7	4.2	2.5
<b>ResUNet</b>	2.3	2.8	2.5	2.8	3.0	2.3	2.3	2.2	1.5	2.8	2.2	3.8	2.2	2.7	3.2	2.3	3.5	1.0	4.2	2.5
<b>VNet</b>	2.7	3.8	3.5	3.0	1.8	2.6	2.7	3.0	2.7	3.3	3.4	3.5	2.2	3.3	3.7	3.2	4.3	1.8	4.4	2.4

#### 4. DISCUSSION

This study shows that while DL segmentation models vary in geometric accuracy, radiomics stability, and predictive performance, their clinical utility becomes comparable once a certain level of reliability and consistency is achieved across these factors. Among the five well-known models, VNet achieved the best testing Dice (0.83) and strong radiomics reproducibility, while SSL with VNet–LASSO–LGBM reached 0.88 accuracy, surpassing SL and underscoring the utility of unlabeled data. ReconNet, despite weaker geometric scores, produced radiomics features with notable prognostic value, and 3D Attention U-Net captured peritumoral heterogeneity most effectively. Still, Friedman tests showed no significant differences for q10 (diagnosis success), q11 (prediction success), or q12 (confidence), indicating that small technical gains did not consistently influence clinical preference. The novel contribution of this work lies in its integrated evaluation framework, which unites geometric metrics, radiomics reproducibility, survival modeling, and physician-centered assessments under the KTA paradigm. We demonstrate that (i) SSL pipelines with VNet can enhance prognostic prediction, (ii) clinical reliability cannot be judged from geometric scores alone but requires outcome-linked metrics and physician input, and (iii) DL segmentation should act as an assistive tool rather than a replacement for clinicians. Physicians further highlighted that AI masks often introduced noisy, unstable boundaries instead of biologically meaningful differences, limiting prognostic stability, and noted that while confidence maps may improve transparency, robust segmentation remains essential.

Physicians' qualitative evaluations provided essential explanatory context for the quantitative findings. AI-generated masks were occasionally judged to be less clinically meaningful than the ground truth, primarily due to inconsistent and noisy boundaries, challenges at spiculated and craniocaudal margins, and geometric instability. These discrepancies seldom corresponded to biologically relevant regions but rather reflected random noise, which likely contributed to the inferior prognostic performance of AI masks compared to ground truth. While AI sometimes captured broader peritumoral regions or additional structures not included in ground truth masks, this was inconsistent and often contaminated with non-tumoral tissue, reducing reliability. Physicians also noted that ground truth segmentations, though occasionally biased by high-contrast thresholds, remained cleaner and more trustworthy. Collectively, these evaluations confirm that current AI delineations introduce instability rather than reliable new information, limiting their direct clinical value.

Within the KTA framework, these findings related to multiple barriers (amongst the 11 barriers to deployment of AI in the clinic as identified in our previous KTA survey study [2]. Section 1 (Overall Impression) reflected clinical skepticism (ii), as physicians judged that AI masks were rarely more meaningful than ground truth, and misregistration undermined confidence. Section 2 (Spatial Differences) addressed adaptability (iii): while VNet and 3D Attention occasionally captured broader peritumoral areas—known to carry prognostic significance—physicians stressed that these regions were captured inconsistently. Section 3 (Tumor Heterogeneity & Boundaries) engaged usability and reliability (vii, xi). Although AI masks sometimes preserve heterogeneity by capturing larger ROIs, this often came at the cost of including irrelevant tissue. Fragmented boundaries resulted in high Hausdorff distances and unstable radiomics features, whereas ground truth contours provided smoother, more reproducible segmentations.

Section 4 (Survival Prediction) aligned with outcome relevance (x). Physicians consistently linked noisy AI boundaries to weaker prognostic stability, confirming that reduced survival prediction performance was caused by unstable tumor representations. While SSL pipelines improved generalization and reduced annotation burden, their success was still dependent on stable segmentation quality. Section 5 (Trust & Preference) highlighted the confidence barrier (iv). Radiologists emphasized that interpretability tools, such as confidence or uncertainty maps, would improve transparency and trust, but they could not compensate for fundamental segmentation errors. Section 6 (Summaries & Assessment) related to standardization (vii). Physicians explicitly rejected Dice/IoU as sufficient measures of trustworthiness, explaining that geometric scores may misrepresent clinical value: models with high scores could still fail at margins, while those with modest scores occasionally captured useful prognostic regions.

Section 7 (Workflow & Adoption) addressed workflow disruption and workforce resistance (vii, viii). Physicians reported that AI masks often increased workload, since noisy and inconsistent boundaries required extensive correction. In some cases, it was easier to redraw from scratch than to refine the AI output. This inefficiency limited adoption despite the technical promise. Moreover, for high-stakes tasks such as radiotherapy planning, even small errors in tumor boundary delineation could compromise staging, surgical margins, or dose delivery. Physicians acknowledged that AI reduced

interobserver variability and could serve as a helpful starting point, but strongly emphasized that its role should remain assistive—providing an initial mask for refinement—rather than autonomous. This mitigates concerns about oversight and job displacement while reinforcing the importance of physician supervision in clinical workflows.

When integrating these findings, VNet emerges as the most suitable model. It not only achieved superior segmentation accuracy and radiomics reproducibility but also aligned best with clinical judgments, offering smoother boundaries, relatively stable peritumoral representation, and greater workflow usability. From a KTA perspective, VNet addresses barriers of infrastructure and integration (i), adaptability (iii), skepticism (ii), trust (iv), reliability (xi), and workflow disruption (vii), making it the most balanced candidate for clinical translation. Furthermore, its role as the backbone of the best-performing SSL pipelines reinforces its value as both a technical and clinically viable solution.

Despite these contributions, limitations remain. Prognostic validation was limited to three datasets, expert evaluation included only six medical professionals, and Likert ratings sometimes revealed ceiling effects. The qualitative assessments were interpretive and highlighted the need for larger, multicenter clinical studies. Ethical, legal, financial, and privacy challenges (v) were not addressed, representing the major unresolved KTA barrier. As a practical next step, we plan to integrate eye-tracking systems into click-point segmentation to enhance usability and reduce user burden, thereby making interactions more intuitive. We will also pilot VNet-based segmentation within real-world clinical workflows, enabling prospective evaluation of usability, physician-AI collaboration, and prognostic value in practice. Larger, multi-institutional studies will be necessary to confirm generalizability, quantify the longitudinal benefits of outcomes, and address the remaining ethical and regulatory challenges.

## 5. CONCLUSION

This study concluded that, although segmentation models differ in geometric accuracy, radiomics stability, and predictive performance, their clinical value becomes comparable once they achieve a sufficient level of consistency and reliability. VNet emerged as the most robust model, achieving superior geometric accuracy (Dice:  $0.83 \pm 0.07$ , IoU:  $0.71 \pm 0.09$ , Hausdorff Distance:  $10.04 \pm 3.73$ ), strong radiomics reproducibility (Spearman Correlation Coefficient = 0.76, ICC = 0.65), and the best predictive performance under SSL (accuracy:  $0.88 \pm 0.003$ , F1:  $0.83 \pm 0.004$ , AUC:  $0.76 \pm 0.048$ , specificity: 1.0). Physician assessments revealed no significant differences in diagnostic or prognostic success among the segmentation methods. However, VNet received higher scores in statistical and radiomics performance, qualitative assessments, segmentation accuracy, and prediction performance, making it particularly favorable for workflow usability. Within the KTA framework, this study tackled 10 of 11 barriers to routine adoption of AI in the clinic. Importantly, the qualitative analysis confirmed that clinicians prefer AI not as a replacement, but as a system that provides an initial mask for refinement or serves as a supportive tool. As part of our future work, we plan to develop a dedicated clinical software platform that integrates VNet-based segmentation with click-point and gaze-tracking functionality, enabling radiologists to intuitively refine AI outputs while minimizing workload. In combination with active learning mechanisms that adapt to physician feedback and embedded predictive/classification pipelines leveraging SSL-derived radiomics, this system aims to streamline segmentation, enhance user trust, and generate prognostically meaningful outputs that can be seamlessly integrated into routine clinical workflows.

## ACKNOWLEDGEMENTS

This study was supported by the Virtual Collaboration Group (VirCollab, [www.vircollab.com](http://www.vircollab.com)) and the Technological Virtual Collaboration (TECVICO CORP.) based in Vancouver, Canada. We gratefully acknowledge funding from the Natural Sciences and Engineering Research Council of Canada (NSERC) Award RGPIN-2023-0357, and Discovery Horizons Grant DH-2025-00119, as well as the UBC Department of Radiology 2023 AI Fund.

## CONFLICT OF INTEREST

Drs. Mohammad R. Salmanpour, Mehdi Maghsudi, Arman Gorji, and Ms. Sonya Falahati are affiliated with TECVICO Corp. The other co-authors declare no relevant conflicts of interest or disclosures.

## DATA AND CODE AVAILABILITY

All code is publicly shared at: <https://github.com/MohammadRSalmanpour/Clinician-in-the-Loop-AI-Segmentation-for-CT-Based-Prognosis/tree/main>

## REFERENCE

1. Liao, X., et al., *Barriers and facilitators to implementing imaging-based diagnostic artificial intelligence-assisted decision-making software in hospitals in China: a qualitative study using the updated Consolidated Framework for Implementation Research*. BMJ Open, 2024. 14(9): p. e084398.

2. A. Fathi Jouzdani, et al., *Crossing the AI Innovation-to-Application Chasm through Implementation Science: Using Concept Mapping in the Knowledge-to-Action Process to Identify and Overcome Barriers to Routine Use of Effective AI in Medical Imaging*. ArXiv, 2025.
3. Hassan, M., A. Kushniruk, and E. Borycki, *Barriers to and Facilitators of Artificial Intelligence Adoption in Health Care: Scoping Review*. JMIR Hum Factors, 2024. 11: p. e48633.
4. Ahmed, M.I., et al., *A Systematic Review of the Barriers to the Implementation of Artificial Intelligence in Healthcare*. Cureus, 2023. 15(10): p. e46454.
5. Ramadan, O.M.E., et al., *Facilitators and barriers to AI adoption in nursing practice: a qualitative study of registered nurses' perspectives*. BMC Nursing, 2024. 23(1): p. 891.
6. Petersson, L., et al., *Challenges to implementing artificial intelligence in healthcare: a qualitative interview study with healthcare leaders in Sweden*. BMC Health Services Research, 2022. 22(1): p. 850.
7. Nair, M., et al., *A comprehensive overview of barriers and strategies for AI implementation in healthcare: Mixed-method design*. PLOS ONE, 2024. 19(8): p. e0305949.
8. Adler-Milstein, J., et al., *Meeting the Moment: Addressing Barriers and Facilitating Clinical Adoption of Artificial Intelligence in Medical Diagnosis*. NAM Perspect, 2022. 2022.
9. Thandria, K.C., et al., *Epidemiology of lung cancer*. Contemp Oncol (Pozn), 2021. 25(1): p. 45-52.
10. Corn, B.W. and D.B. Feldman, *Cancer statistics, 2025: A hinge moment for optimism to morph into hope?* CA: A Cancer Journal for Clinicians, 2025. 75(1): p. 7-9.
11. Gałekci, S., et al. *Assessing the Prognosis of Patients with Metastatic or Recurrent Non-small Cell Lung Cancer in the Era of Immunotherapy and Targeted Therapy*. in *The Latest Developments and Challenges in Biomedical Engineering*. 2024. Cham: Springer Nature Switzerland.
12. Kelly, C.J., et al., *Key challenges for delivering clinical impact with artificial intelligence*. BMC Medicine, 2019. 17(1): p. 195.
13. Aberle, D.R., et al., *The National Lung Screening Trial: overview and study design*. Radiology, 2011. 258(1): p. 243-53.
14. de Koning, H.J., et al., *Reduced Lung-Cancer Mortality with Volume CT Screening in a Randomized Trial*. N Engl J Med, 2020. 382(6): p. 503-513.
15. Facktor, M.A., et al., *Artificial intelligence-aided lung cancer screening in routine clinical practice: A pilot of LungFlag at Geisinger*. Journal of Clinical Oncology, 2024. 42(16\_suppl): p. e13604-e13604.
16. Farsad, M., *FDG PET/CT in the Staging of Lung Cancer*. Curr Radiopharm, 2020. 13(3): p. 195-203.
17. Zhang, Y.-P., et al., *Artificial intelligence-driven radiomics study in cancer: the role of feature engineering and modeling*. Military Medical Research, 2023. 10(1): p. 22.
18. Bagci, U., X. Chen, and J.K. Udupa, *Hierarchical scale-based multiobject recognition of 3-D anatomical structures*. IEEE Trans Med Imaging, 2012. 31(3): p. 777-89.
19. Clèrigues, A., et al., *Acute ischemic stroke lesion core segmentation in CT perfusion images using fully convolutional neural networks*. Comput Biol Med, 2019. 115: p. 103487.
20. Guzene, L., et al., *Assessing Interobserver Variability in the Delineation of Structures in Radiation Oncology: A Systematic Review*. Int J Radiat Oncol Biol Phys, 2023. 115(5): p. 1047-1060.
21. Mehrnia, S.S., et al., *Landscape of 2D Deep Learning Segmentation Networks Applied to CT Scan from Lung Cancer Patients: A Systematic Review*. J Imaging Inform Med, 2025.
22. Yao, I.Z., M. Dong, and W.Y.K. Hwang, *Deep Learning Applications in Clinical Cancer Detection: A Review of Implementation Challenges and Solutions*. Mayo Clinic Proceedings: Digital Health, 2025. 3(3): p. 100253.
23. Traverso, A., et al., *Machine learning helps identifying volume-confounding effects in radiomics*. Phys Med, 2020. 71: p. 24-30.
24. Larue, R.T., et al., *Quantitative radiomics studies for tissue characterization: a review of technology and methodological procedures*. Br J Radiol, 2017. 90(1070): p. 20160665.
25. Alves, N., et al., *Prediction Variability to Identify Reduced AI Performance in Cancer Diagnosis at MRI and CT*. Radiology, 2023. 308(3): p. e230275.
26. Hershman, M., et al., *Impact of Interobserver Variability in Manual Segmentation of Non-Small Cell Lung Cancer (NSCLC) Applying Low-Rank Radiomic Representation on Computed Tomography*. Cancers (Basel), 2021. 13(23).
27. Maier-Hein, L., et al., *Metrics reloaded: recommendations for image analysis validation*. Nat Methods, 2024. 21(2): p. 195-212.
28. Parikh, R.B., Z. Obermeyer, and A.S. Navathe, *Regulation of predictive analytics in medicine*. Science, 2019. 363(6429): p. 810-812.
29. Braman, N.M., et al., *Intratumoral and peritumoral radiomics for the pretreatment prediction of pathological complete response to neoadjuvant chemotherapy based on breast DCE-MRI*. Breast Cancer Research, 2017. 19(1): p. 57.
30. Park, S.H., et al., *Methods for Clinical Evaluation of Artificial Intelligence Algorithms for Medical Diagnosis*. Radiology, 2022. 306(1): p. 20-31.
31. Wang, G., et al., *DeepIGeoS: A Deep Interactive Geodesic Framework for Medical Image Segmentation*. IEEE Trans Pattern Anal Mach Intell, 2019. 41(7): p. 1559-1572.
32. Tschandl, P., et al., *Human-computer collaboration for skin cancer recognition*. Nature Medicine, 2020. 26(8): p. 1229-1234.
33. Zech, J.R., et al., *Variable generalization performance of a deep learning model to detect pneumonia in chest radiographs: A cross-sectional study*. PLOS Medicine, 2018. 15(11): p. e1002683.
34. Ghassemi, M., L. Oakden-Rayner, and A.L. Beam, *The false hope of current approaches to explainable artificial intelligence in health care*. The Lancet Digital Health, 2021. 3(11): p. e745-e750.
35. Lambin, P., et al., *Radiomics: the bridge between medical imaging and personalized medicine*. Nat Rev Clin Oncol, 2017. 14(12): p. 749-762.

36. Mary, M.C.V.S., et al., *An empirical study on optic disc segmentation using an active contour model*. Biomedical Signal Processing and Control, 2015. 18: p. 19-29.

37. Zhang, W. and S. Ray, *From coarse to fine: a deep 3D probability volume contours framework for tumour segmentation and dose painting in PET images*. Frontiers in Radiology, 2023. Volume 3 - 2023.

38. Rayed, M.E., et al., *Deep learning for medical image segmentation: State-of-the-art advancements and challenges*. Informatics in Medicine Unlocked, 2024. 47: p. 101504.

39. Koidala, S.P., et al., *Deep learning based diagnostic quality assessment of choroidal OCT features with expert-evaluated explainability*. Scientific Reports, 2023. 13(1): p. 1570.

40. Salmanpour M. R., et al., *Robust Semi-Supervised CT Radiomics for Lung Cancer Prognosis: Cost-Effective Learning with Limited Labels and SHAP Interpretation*. arXiv:2507.08189, 2025.

41. Yang, J., et al. *Unsupervised Domain Adaptation via Disentangled Representations: Application to Cross-Modality Liver Segmentation*. in *Medical Image Computing and Computer Assisted Intervention – MICCAI 2019*. 2019. Cham: Springer International Publishing.

42. Cheplygina, V., M. de Bruijne, and J.P.W. Pluim, *Not-so-supervised: A survey of semi-supervised, multi-instance, and transfer learning in medical image analysis*. Medical Image Analysis, 2019. 54: p. 280-296.

43. Ibrahim, A., et al., *Radiomics for precision medicine: Current challenges, future prospects, and the proposal of a new framework*. Methods, 2021. 188: p. 20-29.

44. Topol, E.J., *High-performance medicine: the convergence of human and artificial intelligence*. Nature Medicine, 2019. 25(1): p. 44-56.

45. Graham, I.D., et al., *Lost in knowledge translation: time for a map?* J Contin Educ Health Prof, 2006. 26(1): p. 13-24.

46. Bienefeld, N., et al., *Solving the explainable AI conundrum by bridging clinicians' needs and developers' goals*. NPJ Digit Med, 2023. 6(1): p. 94.

47. Berenguer, R., et al., *Radiomics of CT Features May Be Nonreproducible and Redundant: Influence of CT Acquisition Parameters*. Radiology, 2018. 288(2): p. 407-415.

48. Jabbar, Q.A., et al. *Delivering Clinical Impact with AI: Key Challenges and Considerations*. in *2024 International Conference on IoT, Communication and Automation Technology (ICICAT)*. 2024.

49. Pavic, M., et al., *Influence of inter-observer delineation variability on radiomics stability in different tumor sites*. Acta Oncol, 2018. 57(8): p. 1070-1074.

50. Riera-Marín, M., et al., *Calibration and Uncertainty for multiRater Volume Assessment in multiorgan Segmentation (CURVAS) challenge results*. Computers in Biology and Medicine, 2025. 197: p. 111024.

51. Wang, Y., L. Liu, and C. Wang, *Trends in using deep learning algorithms in biomedical prediction systems*. Frontiers in Neuroscience, 2023. Volume 17 - 2023.

52. Yang, G.S., H. Veeraraghavan, E. W. Van , A. Dekker , T. Lustberg and M. Gooding, "Data from Lung CT Segmentation Challenge (LCTSC) (Version 3) [Data set]," 2017. [Online]. Available: <https://www.cancerimagingarchive.net/collection/lctsc/>.

53. Armato III, S.G.H., Lubomir; Tourassi, Georgia D.; Drukker, Karen; Giger, Maryellen L.; Li, Feng; Redmond, George; Farahani, Keyvan; Kirby, Justin S.; Clarke, Laurence P *SPIE-AAPM-NCI Lung Nodule Classification Challenge Dataset*, T.C.I. Archive, Editor. 2015.

54. Madabhushi and M. Rusu, F.R.-P.L.L.-F.-C.-P.V.D.s.T.C.I.A., . Available: <https://www.cancerimagingarchive.net/collection/lung-fused-ct-pathology/>, 2018.

55. O. Grove, A.B., M. Schabath , H. Aerts , A. Dekker, H. Wang, E. Velazquez, P. Lambin, Y. Gu, Y. Balagurunathan and E. Eikman, "Data from: Quantitative computed tomographic descriptors associate tumor shape complexity and intratumor heterogeneity with prognosis in lung adenocarcinoma. The Cancer Imaging Archive.," 2015. [Online]. Available: <https://www.cancerimagingarchive.net/collection/lunget-diagnosis/>.

56. S. Bakr, O.G., S. Echegaray, K. Ayers, M. Zhou, M. Shafiq, H. Zheng, W. Zhang, A. Leung, M. Kadoc and J. Shrager, "Data for NSCLC Radiogenomics (Version 4) [Data set]. The Cancer Imaging Archive.," 2017. [Online]. Available: <https://www.cancerimagingarchive.net/collection/nsclc-radiogenomics/>.

57. H. J. W. L. Aerts , L.W., V. E. Rios, R. T. H. Leijenaar, C. Parmar, P. Grossmann, S. Carvalho, J. Bussink , R. Monshouwer, B. Haibe-Kains and D. Rietveld, "Data From NSCLC-Radiomics (version 4) [Data set]. The Cancer Imaging Archive.," 2014. [Online]. Available: <https://www.cancerimagingarchive.net/collection/nsclc-radiomics/>.

58. H. Aerts, V.E.R., R. Leijenaar, C. Parmar, P. Grossmann, S. Carvalho, J. Bussink, R. Monshouwer, B. Haibe-Kains, D. Rietveld and F. Hoebers, "Data From NSCLC-Radiomics-Genomics. The Cancer Imaging Archive.," 2015. [Online].

59. D. Goldgof, L.H., S. Hawkins, M. Schabath, O. Stringfield, A. Garcia, Y. Balagurunathan, J. Kim, S. Eschrich, A. Berglund and R. Gatenby, "Data From QIN LUNG CT (version 2) [Data set.]," 2015. [Online]. Available: <https://www.cancerimagingarchive.net/collection/qin-lung-ct/>.

60. J. Kalpathy-Cramer, S.N., D. Goldgof and B. Zhao, "QIN multi-site collection of Lung CT data with Nodule Segmentations.," 2015. [Online]. Available: <https://www.cancerimagingarchive.net/collection/qin-lung-ct/>.

61. B. Zhao, L.H.S., M. G. Kris and G. J. Riely, "Coffee-break lung CT collection with scan images reconstructed at multiple imaging parameters (Version 3) [Dataset]. The Cancer Imaging Archive.," 2015. [Online]. Available: <https://www.cancerimagingarchive.net/collection/rider-lung-ct/>.

62. Lung Image Database Consortium, R.P.D.s.T.C.I.A.T., " 2023. [Online]. Available: <https://www.cancerimagingarchive.net/collection/rider-pilot/>.

63. S. G. Armato III, L.H., G. D. Tourassi, K. Drukker, M. L. Giger, F. Li, G. Redmond, K. Farahani, J. S. Kirby and L. P. Clarke, "SPIE-AAPM-NCI Lung Nodule Classification Challenge Dataset. The Cancer Imaging Archive.," 2015. [Online]. Available: <https://www.cancerimagingarchive.net/collection/spie-aapm-lung-ct-challenge/>.

64. B. Albertina, M.W., V. Holback, R. Jarosz, S. Kirk, Y. Lee, K. Rieger-Christ and J. Lemmerman , "The Cancer Genome Atlas Lung Adenocarcinoma Collection (TCGA-LUAD) (Version 4) [Data set].," 2016. [Online].

65. Gao, Y., et al. *Medical Image Segmentation: A Comprehensive Review of Deep Learning-Based Methods*. Tomography, 2025. 11, DOI: 10.3390/tomography11050052.

66. Islam, M., et al. *Brain tumor segmentation and survival prediction using 3D attention UNet*. in *International MICCAI brainlesion workshop*. 2019. Springer.

67. Zhi, L., et al., *Deep neural network pulmonary nodule segmentation methods for CT images: Literature review and experimental comparisons*. Computers in Biology and Medicine, 2023. 164: p. 107321.

68. Milletari, F., N. Navab, and S.A. Ahmadi. *V-Net: Fully Convolutional Neural Networks for Volumetric Medical Image Segmentation*. in *2016 Fourth International Conference on 3D Vision (3DV)*. 2016.

69. Wang, H., et al. *SAM-Med3D: Towards General-Purpose Segmentation Models for Volumetric Medical Images*. in *Computer Vision – ECCV 2024 Workshops*. 2025. Cham: Springer Nature Switzerland.

70. Morteza Alizadeh, M.O., Sonya Falahati, Ghazal Mousavi, Mohsen Alambardar Meybodi, Somayeh Sadat Mehrnia, Ilker Hacihaliloglu, Arman Rahmim, Mohammad R. Salmanpour, *AllMetrics: A Unified Python Library for Standardized Metric Evaluation and Robust Data Validation in Machine Learning*. arXiv:2505.15931, 2025: p. 1-9.

71. Salmanpour, M.R., et al., *Machine Learning Evaluation Metric Discrepancies Across Programming Languages and Their Components in Medical Imaging Domains: Need for Standardization*. IEEE Access, 2025. 13: p. 47217-47229.

72. Salmanpour, M.R., et al. *ViSERA: Visualized & Standardized Environment for Radiomics Analysis - A Shareable, Executable, and Reproducible Workflow Generator*. in *2023 IEEE Nuclear Science Symposium, Medical Imaging Conference and International Symposium on Room-Temperature Semiconductor Detectors (NSS MIC RTSD)*. 2023.

73. Chandrashekhar, G. and F. Sahin, *A survey on feature selection methods*. Computers & Electrical Engineering, 2014. 40(1): p. 16-28.